

Nematic Pairing from Orbital Selective Spin Fluctuations in FeSe

Lara Benfatto,¹ Belén Valenzuela,² and Laura Fanfarillo³

¹ISC-CNR and Department of Physics, “Sapienza” University of Rome, P.le A. Moro 5, 00185, Rome, Italy

²Materials Science Factory, Instituto de Ciencia de Materiales de Madrid, ICMM-CSIC, Cantoblanco, E-28049 Madrid, Spain

³CNR-IOM and International School for Advanced Studies (SISSA), Via Bonomea 265, I-34136, Trieste, Italy*

(Dated: March 16, 2022)

FeSe is an intriguing iron-based superconductor. It presents an unusual nematic state without magnetism and can be tuned to increase the critical superconducting temperature. Recently it has been observed a noteworthy anisotropy of the superconducting gaps. Its explanation is intimately related to the understanding of the nematic transition itself. Here we show that the spin-nematic scenario driven by orbital-selective spin-fluctuations provides a simple scheme to understand both phenomena. The pairing mediated by anisotropic spin modes is not only orbital selective but also nematic, leading to stronger pair scattering across the hole and X electron pocket. The delicate balance between orbital ordering and nematic pairing points also to a marked k_z dependence of the hole-gap anisotropy.

INTRODUCTION

Soon after the discovery of superconductivity in iron-based systems it has been proposed that pairing could be unconventional, i.e. based on a non-phononic mechanism^{1,2}. This proposal has been triggered, from one side, by the small estimated value of the electron-phonon coupling, and, from the other side, by the proximity in the temperature-doping phase diagram of a magnetic instability nearby the superconducting (SC) one. Within an itinerant-electron picture pairing could be provided by repulsive spin-fluctuations (SF) between hole and electron pockets, connected by the same wavevector characteristic of the spin modulations in the magnetic phase (see Fig. 1). This suggestion has been supported and confirmed by an extensive theoretical work, aimed from one side to establish why inter-pockets repulsion can overcome the intra-pocket one³ and from the other side to provide a quantitative estimate of the SC properties starting from RPA-based description of the SF susceptibility^{4,5}.

The success of the itinerant scenario as a unified description of Fe-based materials has been partly questioned by the discovery of superconductivity in the FeSe system. Recent experiments^{6–10} detected sizeable SF in FeSe, however, a magnetic phase appears only upon doping. Superconductivity emerges below $T_c \sim 9$ K from the so-called nematic phase¹¹. Here at temperatures below $T_S = 90$ K the anisotropy of the electronic properties is far larger than what expected across a standard tetragonal-to-orthorhombic transition, suggesting that it is driven by electronic degrees of freedom^{11,12}. In particular, ARPES experiments clearly show a dramatic change of the Fermi surface (FS) across T_S , that can be reproduced with an effective crystal-field splitting of the various orbitals^{13–21}.

In this situation, the explanation of the observed anisotropy of the SC gaps in FeSe becomes intimately related to the understanding of the nematic transition itself. Extensive experimental studies on FeSe-based mate-

rial, ranging from quasiparticle interference imaging^{22,23} and ARPES measurements^{24–28}, to thermal probes^{29,30}, suggest that the SC gap in FeSe is highly anisotropic on both hole and electron pockets. By defining θ the angle formed with the k_x axis measured with respect to the center of each pocket, one finds that the gap is larger at $\theta = 0$ on the Γ pocket, where the predominant character in the nematic phase is xz ^{19,26,27}, and at $\theta = \pi/2$ on the X pocket, where the dominant character is yz , Fig. 1b. Thus, accounting for an orbital-dependent SC order parameter does not reproduce the observed gap hierarchy, and additional phenomenological modifications of the pairing mechanism must be introduced^{22,26,31} to describe the experiments.

Among the various attempts to theoretically understand the nematic phase from microscopic models, we have recently emphasized the outcomes of a theoretical approach which correctly incorporates the feedback between orbital degrees of freedom and SF^{19,32,33}. From

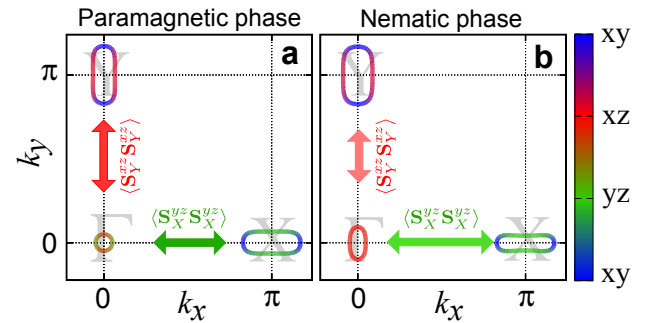


FIG. 1: FeSe Fermi surfaces at $k_z = 0$. (a) Paramagnetic phase. (b) Nematic phase. The colors represent the main orbital character of the Fermi surface. The green/red arrows denote the orbital selective spin fluctuations (OSSF), connecting hole and electron pockets at different momenta, see Eq. (6)-(43). The spin-fluctuations along ΓX and ΓY are equivalent in the paramagnetic phase (a) and become anisotropic in the nematic one (b)

one side the degree of orbital nesting between hole and electron pockets is crucial to determine the temperature scale where SF beyond RPA drive the spin-nematic instability³², making SF at $\mathbf{Q}_X = (\pi/a, 0)$ and $\mathbf{Q}_Y = (0, \pi/a)$ anisotropic below T_S ³⁴. From the other side SF renormalize the quasiparticle dispersion, so that the orbital ordering observed below T_S is a consequence of the spin nematicity, thanks to an orbital-selective shrinking mechanism¹⁹. In this work we show that such orbital-selective spin fluctuations (OSSF) provide also the key pairing mechanism needed to understand the SC properties of FeSe. Within an orbital-selective spin-nematic scenario, the C_4 symmetry breaking of the SF below T_S provides a pairing mechanism that is not only orbital selective but also nematic, in the sense that inter-pocket pair scattering along the ΓX and ΓY directions becomes anisotropic. As we show below, accounting only for the nematic band-structure reconstruction of the FS, the SC gap of the Γ pocket follows the modulation of the dominant xz orbital, with a weak relative maximum at $\theta = \pi/2$, in striking disagreement with the experiments. The nematic pairing provided by OSSF is crucial to enhance the yz component of the SC order parameter, explaining why the anisotropy of the SC gap at Γ follows the subdominant yz orbital character of the underlying Fermi surface^{26,27}. We also discuss its implications for the gap-structure measured at $k_z = \pi$ (ref.s 24,25,28), where hole pocket retains a larger yz character even in the nematic phase, making the nematic pairing responsible for an enhancement of the moderate gap anisotropy triggered already by orbital-ordering effects³⁵.

RESULTS

Model

To compute the SC properties of FeSe we start from a low-energy model adapted from³⁶. The orbital content of each pocket is encoded via a rotation from the fermionic operators c_{xz}, c_{yz}, c_{xy} in the orbital basis to the ones describing the outer hole pocket (h) at Γ and the electronic pockets at X (e_X) and at Y (e_Y):

$$h_{\mathbf{k}} = u_{\Gamma, \mathbf{k}} c_{yz, \mathbf{k}} - v_{\Gamma, \mathbf{k}} c_{xz, \mathbf{k}}, \quad (1)$$

$$e_{X, \mathbf{k}} = u_{X, \mathbf{k}} c_{yz, \mathbf{k}} - i v_{X, \mathbf{k}} c_{xy, \mathbf{k}}, \quad (2)$$

$$e_{Y, \mathbf{k}} = u_{Y, \mathbf{k}} c_{xz, \mathbf{k}} - i v_{Y, \mathbf{k}} c_{xy, \mathbf{k}}, \quad (3)$$

where the explicit definition of the coefficients $u_{\ell, \mathbf{k}}, v_{\ell, \mathbf{k}}$ with $\ell = \Gamma, X, Y$ is given in Supplementary Note 1. For example, for the hole pocket in the tetragonal phase $u_{\Gamma, \mathbf{k}_F} \sim \cos \theta$ and $v_{\Gamma, \mathbf{k}_F} \sim \sin \theta$, accounting for the pre-dominant orbital character of the FS represented in Fig. 1a. By using the identities (1)-(3) one can establish^{32,37} (see also Supplementary Note 2) a precise correspondence between the orbital character of the spin operator and the momenta \mathbf{Q}_X or \mathbf{Q}_Y connecting the hole and the X/Y

pockets:

$$\mathbf{S}(\mathbf{Q}_X) \equiv \mathbf{S}_X^{yz} = \sum_{\mathbf{k}} u_{\Gamma, \mathbf{k}} h_{\mathbf{k}}^\dagger \vec{\sigma} u_{X, \mathbf{k}+\mathbf{Q}_X} e_{X, \mathbf{k}+\mathbf{Q}_X}, \quad (4)$$

$$\mathbf{S}(\mathbf{Q}_Y) \equiv \mathbf{S}_Y^{xz} = \sum_{\mathbf{k}} -v_{\Gamma, \mathbf{k}} h_{\mathbf{k}}^\dagger \vec{\sigma} u_{Y, \mathbf{k}+\mathbf{Q}_Y} e_{Y, \mathbf{k}+\mathbf{Q}_Y}. \quad (5)$$

Since xz states are absent at X the $S_{\mathbf{q}}^{xz}$ operator has no component at the wavevector \mathbf{Q}_X connecting the Γ and X pocket, and viceversa for the yz states. This leads to OSSF at different momenta, as depicted in Fig. 1:

$$\langle \mathbf{S} \cdot \mathbf{S} \rangle(\mathbf{Q}_X) \Rightarrow \langle \mathbf{S}_X^{yz} \cdot \mathbf{S}_X^{yz} \rangle, \quad (6)$$

$$\langle \mathbf{S} \cdot \mathbf{S} \rangle(\mathbf{Q}_Y) \Rightarrow \langle \mathbf{S}_Y^{xz} \cdot \mathbf{S}_Y^{xz} \rangle. \quad (7)$$

The existence of OSSF provides a natural explanation of the orbital ordering observed in the nematic phase of FeSe. In fact, the self-energy corrections due to spin exchange imply a shift in the chemical potential with opposite sign for the hole and electron pockets, leading in both cases to a shrinking of the FS^{19,38} that explains why experimentally they are always smaller than LDA predictions^{19,39,40}. Within the OSSF model, due to the orbital-selective nature of SF, this mechanism is also orbital dependent¹⁹. As a consequence, within a spin-nematic scenario, the C_4 symmetry breaking of SF along ΓX and ΓY explains also the orbital ordering observed in the nematic phase. It has been shown¹⁹ that, by assuming stronger SF at \mathbf{Q}_X below T_S , the self-energy difference $\Delta\Sigma$ between xz and yz and orbitals induced an orbital splitting being positive at Γ and negative at the electron pockets, leading to the observed deformations of the FS below T_S ^{11,15,17,19-21}. Even though this orbital-selective shrinking mechanism is generic, its effect can be quantitatively different in the various family of iron-based superconductors. For example, in the 122 family the survival of the inner hole pocket enhances the degree of orbital nesting between hole and electron pockets favoring magnetism, this explains why in 122 the nematic transition is immediately followed by the magnetic one³². The quantitative determination of the nematic splitting induced by the nematic spin modes requires a direct comparison with the low-energy band dispersion, as done explicitly for FeSe in¹⁹. Here we take these results for granted and we start from a low-energy model that includes already the effective masses, isotropic shrinking and nematic splittings needed to reproduce the ARPES FS measured in the nematic phase above T_c , and the k_z dependence of the hole pocket between the Γ ($k_z = 0$) and Z ($k_z = \pi$) point (see Supplementary Note 3). The resulting FS at $k_z = 0$ is shown in Fig. 1.

The effect of the nematic orbital splitting on the orbital factors below T_S is shown in Fig. 2. Here, $\Delta\Sigma_h = (\Sigma_{xz}^\Gamma - \Sigma_{yz}^\Gamma)/2$ denotes the nematic splitting at Γ and $\Delta\Sigma_e = (\Sigma_{yz}^X - \Sigma_{xz}^Y)/2$ is the nematic splitting at $M = (X, Y)$ with $\Sigma_{yz/xz}^\ell$ being the yz/xz orbital component of the real part of the self-energy for the ℓ pocket (see Supplementary Note 1). The maximum values are chosen to match the experimental ones^{11,19-21},

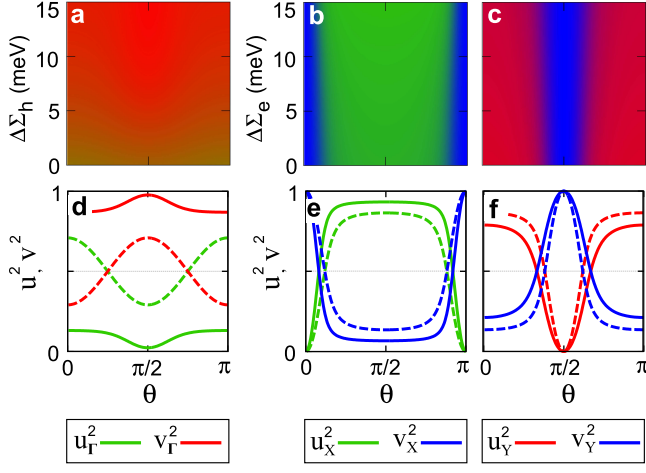


FIG. 2: Orbital content of the FS. (a-c) Color maps of the orbital content of the Γ (a), X (b), Y (c) pockets FS as a function of the angle and of the nematic splitting $\Delta\Sigma_{h/e}$. The color code is the same as in Fig. 1. (d-f) Orbital content of the same pockets as a function of θ at $\Delta\Sigma_{h/e} = 0$, i.e. in the tetragonal phase (dashed lines) and in the nematic phase $\Delta\Sigma_{h/e} = 15$ meV (solid lines).

i.e. $\Delta\Sigma_{h/e} \simeq 15$ meV. The most dramatic changes due to the nematic order are found in the orbital occupation of the hole pocket Fig. 2a,d. The presence of a relatively large spin-orbit coupling ($\simeq 20$ meV) implies a mixing of the xz and yz orbitals on all the FS. However, below T_S the yz character of the hole pocket is strongly suppressed, and the pocket acquires a dominant xz character even at $\theta = 0$, as observed by the polarization dependent ARPES measurements^{17,19,26,27}. At the same time the nematic splitting enhances the yz occupation at X (Fig. 2b,e), and suppresses the xz at Y (Fig. 2c,f). As a consequence, one easily understands that considering the orbital character of the SC order parameter is not enough to explain the observed gap hierarchy. In fact, on the X pocket the gap is maximum at $\theta = \pi/2$, where the band has strong yz character, while on the Γ pocket it is larger at $\theta = 0$, where a dominant xz character is found. The crucial ingredient required to account for the SC properties of FeSe comes indeed from the nematic pairing provided by OSSF, as we show below.

By building up the spin-singlet vertex mediated by the SF (6)-(43) one obtains (see Supplementary Note 2) a pairing Hamiltonian involving only the xz/yz orbital sector:

$$H_{\text{pair}}^{xz,yz} = -g_X \sum_{\mathbf{k},\mathbf{k}'} u_{\Gamma,\mathbf{k}}^2 h_{\mathbf{k}}^\dagger h_{-\mathbf{k}}^\dagger u_{X,\mathbf{k}'}^2 e_{X,-\mathbf{k}'} e_{X,\mathbf{k}'} - g_Y \sum_{\mathbf{k},\mathbf{k}'} v_{\Gamma,\mathbf{k}}^2 h_{\mathbf{k}}^\dagger h_{-\mathbf{k}}^\dagger v_{Y,\mathbf{k}'}^2 e_{Y,-\mathbf{k}'} e_{Y,\mathbf{k}'} + h.c. \quad (8)$$

The coefficients $u_{\ell,\mathbf{k}}$, $v_{\ell,\mathbf{k}}$, accounting for the pockets orbital character, preserve the C_4 band-structure symmetry above T_S and reproduce the nematic reconstruction below T_S . The $g_{X/Y}$ couplings control the strength of the pair hopping between the Γ and X/Y pockets. Within

a spin-nematic scenario, OSSF below T_S are stronger along ΓX than along ΓY leading to a *nematic pairing anisotropy* with $g_X > g_Y$. Within the present itinerant-fermions picture the SF are peaked at the wavevectors connecting hole-like with electron-like pockets. Thus, due to the absence in FeSe of the hole-like xy band at Γ one can neglect the spin-mediated pairing in the xy channel. However, SF at RPA level were found³¹ to be most prominent at $\mathbf{Q} = (\pi, \pi)$. While this could be consistent with inelastic neutron scattering measurements at high temperatures, it does not account for the predominance of stripe-like SF at $(\pi, 0)$ in the nematic phase⁷. In addition, a predominant $\mathbf{Q} = (\pi, \pi)$ pairing channel implies a maximum gap value on the xy sector of the electron pocket, that is in sharp contrast with the experiments. This led the authors of refs.^{22,31} to phenomenologically introduce orbital-dependent spectral weights to suppress this channel (see Discussion section). In general, one can still expect that a smaller pair hopping between the X, Y pockets is present in the xy sector. For the sake of completeness, and with the aim of reducing the number of free parameters, we considered also in this case only an interband xy pairing term, acting between the two electron-like pockets:

$$H_{\text{pair}}^{xy} = -g_{xy} \sum_{\mathbf{k},\mathbf{k}'} v_{X,\mathbf{k}}^2 e_{X,\mathbf{k}}^\dagger e_{X,-\mathbf{k}}^\dagger v_{Y,\mathbf{k}'}^2 e_{Y,-\mathbf{k}'} e_{Y,\mathbf{k}'} + h.c. \quad (9)$$

The set of Eq.s (8)-(9) is solved in the mean-field approximation by defining the orbital-dependent SC order parameters for the hole ($\Delta_h^{yz}, \Delta_h^{xz}$) and electron ($\Delta_e^{yz}, \Delta_e^{xz}, \Delta_X^{xy}, \Delta_Y^{xy}$) pockets. The self-consistent equations at $T = 0$ reads:

$$\Delta_h^{yz} = -g_X \sum_{\mathbf{k}} u_{X,\mathbf{k}}^2 (u_{X,\mathbf{k}}^2 \Delta_e^{yz} + v_{X,\mathbf{k}}^2 \Delta_X^{xy}) / E_{X,\mathbf{k}} \quad (10)$$

$$\Delta_h^{xz} = -g_Y \sum_{\mathbf{k}} u_{Y,\mathbf{k}}^2 (u_{Y,\mathbf{k}}^2 \Delta_e^{xz} + v_{Y,\mathbf{k}}^2 \Delta_Y^{xy}) / E_{Y,\mathbf{k}} \quad (11)$$

$$\Delta_e^{yz} = -g_X \sum_{\mathbf{k}} u_{\Gamma,\mathbf{k}}^2 (u_{\Gamma,\mathbf{k}}^2 \Delta_h^{yz} + v_{\Gamma,\mathbf{k}}^2 \Delta_h^{xz}) / E_{\Gamma,\mathbf{k}} \quad (12)$$

$$\Delta_e^{xz} = -g_Y \sum_{\mathbf{k}} v_{\Gamma,\mathbf{k}}^2 (u_{\Gamma,\mathbf{k}}^2 \Delta_h^{yz} + v_{\Gamma,\mathbf{k}}^2 \Delta_h^{xz}) / E_{\Gamma,\mathbf{k}} \quad (13)$$

$$\Delta_X^{xy} = -g_{xy} \sum_{\mathbf{k}} v_{Y,\mathbf{k}}^2 (u_{Y,\mathbf{k}}^2 \Delta_e^{xz} + v_{Y,\mathbf{k}}^2 \Delta_Y^{xy}) / E_{Y,\mathbf{k}} \quad (14)$$

$$\Delta_Y^{xy} = -g_{xy} \sum_{\mathbf{k}} v_{X,\mathbf{k}}^2 (u_{X,\mathbf{k}}^2 \Delta_e^{xz} + v_{X,\mathbf{k}}^2 \Delta_X^{xy}) / E_{X,\mathbf{k}} \quad (15)$$

Here $E_{\ell,\mathbf{k}} = \sqrt{\varepsilon_{\ell,\mathbf{k}}^2 + \Delta_{\ell,\mathbf{k}}^2}$ is the dispersion in the SC state, where $\varepsilon_{\ell,\mathbf{k}}$ is the band dispersion on each pocket $\ell = \Gamma, X, Y$ above T_c and $\Delta_{\ell,\mathbf{k}}$ is the band gap defined as:

$$\Delta_{\Gamma,\mathbf{k}} = u_{\Gamma,\mathbf{k}}^2 \Delta_h^{yz} + v_{\Gamma,\mathbf{k}}^2 \Delta_h^{xz}, \quad (16)$$

$$\Delta_{X,\mathbf{k}} = u_{X,\mathbf{k}}^2 \Delta_e^{yz} + v_{X,\mathbf{k}}^2 \Delta_X^{xy}, \quad (17)$$

$$\Delta_{Y,\mathbf{k}} = u_{Y,\mathbf{k}}^2 \Delta_e^{xz} + v_{Y,\mathbf{k}}^2 \Delta_Y^{xy}. \quad (18)$$

Superconducting Gaps Anisotropy

The overall momentum dependence of the band gaps is determined by the interplay between the momentum dependence of the orbital factors and the hierarchy of the orbital SC order parameters. In the absence of nematic order Eq.s (10)-(18) preserve the symmetry in the exchange of the xz/yz orbitals. Thus $\Delta_h^{xz} = \Delta_h^{yz}$ and the gap on the Γ pocket Eq. (16) is constant, since $u_{\Gamma,\mathbf{k}}^2 + v_{\Gamma,\mathbf{k}}^2 = 1$. In the nematic state the band structure breaks the C_4 symmetry, making $v_{\Gamma,\mathbf{k}}^2 \gg u_{\Gamma,\mathbf{k}}^2$ (see Fig. 2d), and also the SC orbital parameters Δ_h^{xz} and Δ_h^{yz} are in general different. However, as we shall see below, for isotropic pairing $g_X = g_Y$ the gaps anisotropy is the wrong one. The experimentally-observed anisotropy can only be achieved making $\Delta_{yz}^h \gg \Delta_{xz}^h$, that follows from the nematic pairing mechanism $g_X > g_Y$ provided by spin-nematic OSSF.

To understand the effect of the band-structure nematic reconstruction on the SC gap anisotropy we show in Fig. 3 the evolution of the orbital-factors overlaps appearing in Eq.s (10)-(13), where we define the angular average of a given function as $\langle f(\mathbf{k}) \rangle \equiv \int d\theta / (2\pi) f(k_F(\theta))$, with $k_F(\theta)$ FS wavevector of a given pocket. We can in first approximation neglect the pairing in the subleading xy channel and consider only what happens in the xz/yz orbital sector. As mentioned above, the nematic splitting on the electron pockets leads to a moderate enhancement of the yz factor appearing in Eq. (10) with respect to the xz in Eq. (11), i.e $\langle u_X^4 \rangle \gtrsim \langle u_Y^4 \rangle$, Fig. 3b. This effect, recently highlighted while discussing the $k_z = \pi$ FS cut³⁵, is however too small to account for the observed hole-gap anisotropy at $k_z = 0$. In fact, the strong modification of the hole-pocket orbital factors implies that $\langle u_{\Gamma}^4 \rangle \ll \langle u_{\Gamma}^2 v_{\Gamma}^2 \rangle < \langle v_{\Gamma}^4 \rangle$, Fig. 3a. Thus, by neglecting logarithmic corrections in the gap ratios, from Eq.s (10)-(13)

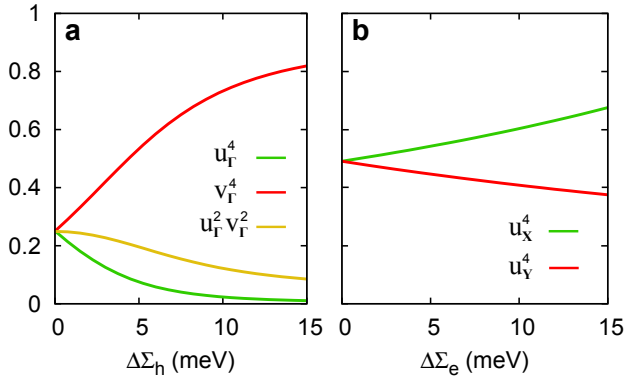


FIG. 3: Angular-averaged orbital-weight overlaps. (a,b) Nematic-splitting dependence of the angular-averaged orbital-weight overlaps appearing in the SC gap equations Eq.s (10)-(13).

one obtains that

$$\frac{\Delta_e^{yz}}{\Delta_e^{xz}} \simeq \frac{g_X}{g_Y} \frac{\langle u_{\Gamma}^2 v_{\Gamma}^2 \rangle}{\langle v_{\Gamma}^4 \rangle} \simeq 0.1 \frac{g_X}{g_Y} \quad (19)$$

and

$$\frac{\Delta_h^{yz}}{\Delta_h^{xz}} \simeq \frac{g_X}{g_Y} \frac{\langle u_X^4 \rangle}{\langle u_Y^4 \rangle} \frac{\Delta_e^{yz}}{\Delta_e^{xz}} \simeq 1.8 \frac{g_X}{g_Y} \frac{\Delta_e^{yz}}{\Delta_e^{xz}}. \quad (20)$$

Note that Eq.s(19)-(20) are almost unaffected once the xy pairing channel is taken into account. From Eq.s(19)-(20) it follows that an isotropic pairing interaction $g_X = g_Y$ (as considered in ref. 35) would lead to a suppression of the yz gap parameters. At the Γ pocket, where the yz orbital character is also strongly suppressed by nematicity ($u_{\Gamma}^2 \ll v_{\Gamma}^2$, Fig. 3a), the band gap would have only xz character, $\Delta_{\Gamma,\mathbf{k}} \simeq \Delta_h^{xz} v_{\Gamma,\mathbf{k}}^2$, leading to a small modulation with a relative maximum at $\theta = \pi/2$ (dashed line in Fig. 3a), in contrast with the experimental findings. On the other hand, the OSSF-mediated anisotropic pairing with $g_X/g_Y \gg 1$ gives a substantial *enhancement*

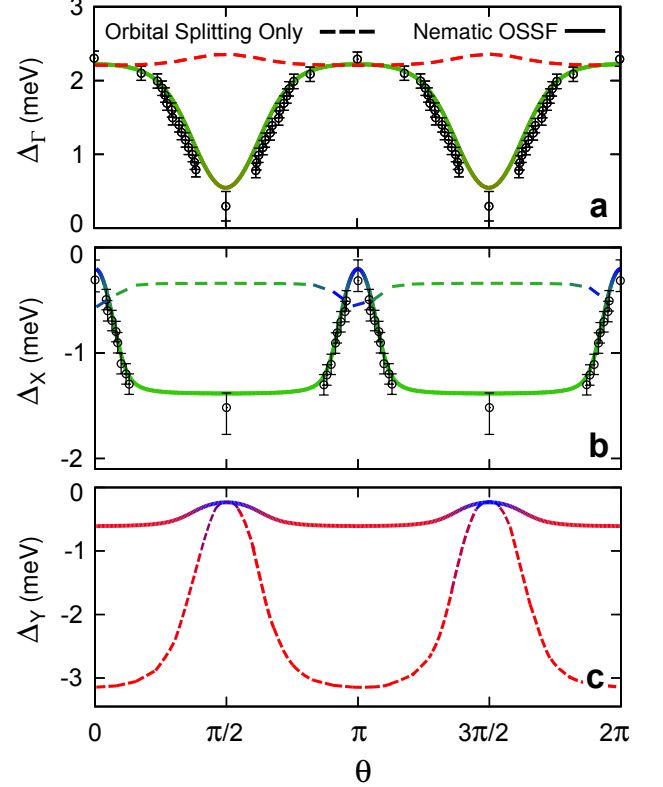


FIG. 4: Angular dependence of the SC band gaps. (a) SC gap on the hole, (b) on the X electron pocket, (c) on the Y electron pocket. Dashed lines are the results for the isotropic pairing $g_X/g_Y = 1$, while solid line for nematic pairing $g_X/g_Y \sim 21$. The color code accounts for the orbital component of the SC gap (green yz , red xz , blue xy), given by the product of the SC orbital parameter and the orbital weight, according to the definitions (16)-(18). For comparison we reproduce the experimental gap values with standard deviations from ref. 22 (black circles).

of the $\Delta_h^{yz}/\Delta_h^{xz}$ ratio. This leads to $\Delta_{\Gamma,\mathbf{k}} \simeq \Delta_h^{yz} u_{\Gamma,\mathbf{k}}^2$, in agreement with the band-gap anisotropy observed experimentally as shown in Fig. 4a, where the numerical solutions of Eq.s (10)-(13) are reported along with the experimental data of²². Here the colour code does not refer to the orbital content of the pocket, as in Fig. 1, but to the orbital content of the SC gap function, that is determined by the product of the SC order parameter times the orbital weight in each sector, Eq.s (16)-(18).

The anisotropy $g_X/g_Y = 21$ extracted from this analysis is rather large, since one needs to overcome the strong suppression of the yz orbital due to nematic reconstruction at the hole pocket: one needs at least $g_X/g_Y \gtrsim 2$ (not shown) to start to see the correct symmetry of the gap at Γ , i.e. a maximum at $\theta = 0$. The value of g_X/g_Y obtained by the SC-gaps analysis is compatible with the anisotropy of the OSSF used to reproduce the orbital selective shrinking of the FS in the nematic phase¹⁹ as discussed in Supplementary Note 3. In principle, the nematic-pairing anisotropy could also be estimated by the direct measurements of the SF. However, while it has been established that in the nematic phase SF are stronger at $(\pi, 0)$ than at (π, π) ⁶⁻⁸, the different intensity expected at $(\pi, 0)$ and $(0, \pi)$ has not been measured yet in detwinned samples.

The gap obtained for the X pocket is shown in Fig. 4b. Its value is also in overall in agreement with the STM experimental data²². To reproduce the experimental value of the xy component we needed a small ($|g_{xy}| \ll g_X$) attractive interband interaction between the two electron-like pockets. In fact, a negative g_{xy} guarantees, from Eq.s (14)-(15), that the SC xy order parameters on both electron pockets have the opposite sign with respect to the one at the hole pockets, as required by the dominant spin-mediated channel. In contrast, a repulsive g_{xy} induces a frustration that turns out in a gap with nodes along the Fermi surface⁴¹. Even though this has been recently suggested by specific-heat measurements⁴², the STM data²² shown for comparison exclude the presence of nodes and force us to consider a negative g_{xy} . It is important to stress that, even though the full set of equations (10)-(15) must be solved self-consistently, adding or not the xy channel is not relevant for what concerns the understanding of the gap behavior in the xz/yz sector, especially for the gap anisotropy at the Γ pocket. For the sake of completeness we report in Fig. 4c also the gap on the Y pocket, that has not been resolved so far in STM²². As one can see, for the electronic pockets an isotropic pairing $g_X = g_Y$ would lead to a strong difference between the absolute gap values at X and Y , due to the effect of nematic ordering at the electronic pockets, as one understands from Eq. (19) above. In contrast nematic pairing leads to more similar gap values, which can be hardly disentangled experimentally, explaining why recent ARPES results claiming to resolve the Y pocket do not report appreciable significant gap differences on the two electron pockets²⁸. The differences between the X and Y gaps due to the nematic pairing could how-

ever have implications for the thermal probes sensibles to single-particle excitations. We leave the analysis of those effects for future work.

Recently, the k_z -dependence of the gap anisotropy on the hole pocket has been investigated²⁸, and it has been shown that the $\Delta_{\Gamma}(\theta = 0)/\Delta_{\Gamma}(\theta = \pi/2)$ anisotropy increases as one moves from the $k_z = 0$ to the $k_z = \pi$ cut. Even though we did not consider a full 3D model, this effect can be understood by considering the variations of the hole-pocket orbital content when moving from $k_z = 0$ to $k_z = \pi$ (Z point). The larger size of the hole pocket at Z makes its orbital content less sensitive to nematic ordering and spin-orbit mixing, so that it still preserves a marked yz character around $\theta = 0$ (ref.s 24,25,35), with $u_{\Gamma} \sim \cos \theta$ and $v_{\Gamma} \sim \sin \theta$ also in the nematic phase (Fig. 5a). In this situation $\langle u_{\Gamma}^4 \rangle \sim \langle v_{\Gamma}^4 \rangle$ so that the enhancement $\langle u_X^4 \rangle > \langle u_Y^4 \rangle$ of the orbital factors in the electron pockets is enough to guarantee that $\Delta_h^{yz} > \Delta_h^{xz}$, leading to a hole-pocket gap anisotropy compatible with the measurements even when $g_X = g_Y$, as recently shown in³⁵ (dashed line Fig. 5b). On the other hand, by retaining the same ratio g_X/g_Y extracted from the $k_z = 0$ gap fit (solid line Fig. 5b), we find an increase of the anisotropy when moving from the Γ to the Z pocket. While this is consistent with the observations in pure²⁸ and S-doped²⁴ FeSe, other groups^{25,26} report instead an overall smaller gap at $k_z = 0$. The analysis of SC fluctuations above T_c , could provide an alternative experimental test to clarify the 3D behavior. As shown in⁴³, the crossover from 2D to 3D character of the fluctuation contribution to the paraconductivity is controlled by the k_z dependence of the pairing interactions. This effect, used to explain the measurements in 122 systems⁴⁴, could be tested in FeSe as well.

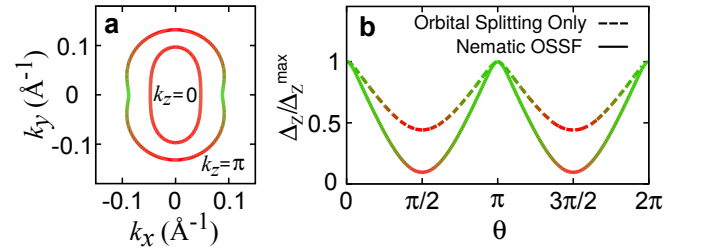


FIG. 5: FS and SC gap for the hole pocket at $k_z = \pi$. (a) FS at $k_z = 0$ and $k_z = \pi$ in the nematic phase. At $k_z = \pi$ the hole pocket retains a full yz orbital character at $\theta = 0$. (b) Angular dependence of the SC gap Δ_Z renormalized to its maximum value obtained using the same g_X/g_Y extracted from the $k_z = 0$ gap fit (see Supplementary Note 3). Same color code of Fig. 4. The Δ_Z maximum at $\theta = 0$ is obtained already for isotropic pairing $g_X = g_Y$ (dashed lines), see also³⁵. The nematic pairing (solid lines) further enhances the gap anisotropy, leading to larger relative variations on the Z pocket, in agreement with ARPES experiments²⁸

DISCUSSION

The C_4 symmetry breaking of paramagnetic SF is a consequence of SF interactions beyond RPA^{32,34}. As a consequence the effects of the nematic SF pairing $g_X > g_Y$ highlighted in the present work cannot be captured by microscopic models where the SF are described at RPA level, even when RPA fluctuations are computed using the nematic reconstruction of the band structure^{31,45}. An alternative route followed in^{22,31} amounts to start from band dispersions fitted to ARPES data and to account phenomenologically for the role of correlations. The so-called orbital differentiation of the electronic mass renormalization due to local electronic interactions has been studied in DMFT-like calculations in the tetragonal phase^{46,47}, which found in particular a larger renormalization of the xy orbital with respect to the xz/yz ones. In addition, correlations can also cooperate to enhance the xz/yz orbital differentiation induced by other nematic mechanisms⁴⁸. Inspired by these results, the authors of ref.s 22,31 added phenomenologically orbital-dependent quasiparticle spectral weights, Z_{orb} , in the RPA-based calculation of the pairing interaction. By using $Z_{xy} \ll Z_{xz} < Z_{yz}$ they obtain the twofold result to make the Y pocket incoherent, explaining why it does not show up in the STM analysis^{22,49}, and to move the maximum of SF from $\mathbf{Q} = (\pi, \pi)$ to $\mathbf{Q} = \mathbf{Q}_X$ ⁴⁵, explaining the neutron-scattering experiments^{7,8} and the observed gap hierarchy. However, this approach presents some inconsistencies. One issue is methodological: by using independent parameters to renormalize the band structure (that is fitted from the experiments) and to define the residua of the Green's functions, one misses the strict relation between these two quantities. On the other hand, by implementing this relation self-consistently, as done for example in⁵⁰, it is not obvious how one can reconcile the large Fermi-velocity anisotropy implicit in the $Z_{xz} < Z_{yz}$ relation with the experimental band structure, that is well reproduced accounting only for a crystal-field splitting of the tetragonal band structure having $Z_{xz} = Z_{yz}$ ^{11,26,27}. A second issue arises by the comparison with experiments. The route followed in^{22,31} is equivalent to rewrite the SC gap e.g. on the Γ pocket as:

$$\Delta_{\Gamma, \mathbf{k}} = Z_{yz} u_{\Gamma, \mathbf{k}}^2 \Delta_h^{yz} + Z_{xz} v_{\Gamma, \mathbf{k}}^2 \Delta_h^{xz} \quad (21)$$

In our case, Eq. (16), the predominance of the SC yz orbital component is achieved via $\Delta_{yz}^h \gg \Delta_{xz}^h$, as guaranteed by the nematic-pairing condition $g_X \gg g_Y$. Instead in Eq. (21) this is due mainly to the rescaling of the orbital occupation factors by the corresponding spectral weights $Z_{yz/xz}$. By assuming $Z_{yz} \gg Z_{xz}$ ^{22,31} one finds $\Delta_{\Gamma, \mathbf{k}} \simeq Z_{yz} u_{\Gamma, \mathbf{k}}^2 \Delta_h^{yz}$, consistently with the measured gap anisotropy. However, the rescaling of the yz orbital occupation to $Z_{yz} u_{\Gamma, \mathbf{k}}^2$ is operative not only on the SC gap function, but also on the band structure above T_c . This restores the yz character of the Γ pocket⁴⁵, in contrast with ARPES measurements which clearly indicate^{26,27} its predominant xz character.

To reconcile ARPES with RPA-based calculations of the spin-mediated pairing interactions the authors of²⁶ use the alternative approach to remove intentionally the contribution of the Y pocket from the RPA-mediated pairing interaction. This is equivalent to put $g_Y = 0$ in Eq.s (10)-(13), so that $\Delta_h^{xz} = 0$ and the modulation of the gap at Γ follows again the yz orbital weight, even if it is largely subdominant. With respect to these approaches, the main advantage of our model is to provide, via the orbital selectivity of the OSSF, a mechanism able to achieve the $g_X > g_Y$ nematic pairing without affecting strongly the quasiparticle spectral weights, while a main disadvantage is the lack of a theoretical justification for the missing Y pocket. However, we cannot help noticing that this point is also controversial from the experimental point of view, due to different reports claiming to observe^{19,28} or not^{22,26} the Y pocket.

In summary, our work provides a paradigm for the emergence of superconductivity in FeSe from an orbital-selective nematic SF mechanism. By combining the orbital ordering induced by the nematic shrinking of the Fermi surface pockets below the nematic transition with the anisotropic pairing interaction mediated by nematic SF, we explain the gap hierarchy reported experimentally on hole and electron pockets, and its variation with k_z . Our findings offer also a fresh perspective on previous attempts to explain the SC properties of FeSe, highlighting from one side the crucial role of spin-mediated pairing, and from the other side clarifying the importance of spin-spin interactions beyond RPA level. This result represents then a serious challenge for a full microscopic approach, that must account self-consistently for the emergence of Ising-nematic SF below the nematic transition temperature.

METHODS

Pairing by Orbital selective spin fluctuations

The mean-field equations for the pairing Hamiltonian, Eq.s (8)-(9), can be easily derived by defining the orbital-dependent SC order parameters for the hole ($\Delta_h^{yz}, \Delta_h^{xz}$) and electron ($\Delta_e^{yz}, \Delta_e^{xz}$) pockets as:

$$\Delta_e^{yz} = -g_X \langle u_{\Gamma, \mathbf{k}}^2 h_{\mathbf{k}} h_{-\mathbf{k}} \rangle, \quad (22)$$

$$\Delta_e^{xz} = -g_Y \langle v_{\Gamma, \mathbf{k}}^2 h_{\mathbf{k}} h_{-\mathbf{k}} \rangle, \quad (23)$$

$$\Delta_h^{yz} = -g_X \langle u_{Y, \mathbf{k}}^2 e_{Y, \mathbf{k}} e_{Y, -\mathbf{k}} \rangle, \quad (24)$$

$$\Delta_h^{xz} = -g_Y \langle u_{Y, \mathbf{k}}^2 e_{Y, \mathbf{k}} e_{Y, -\mathbf{k}} \rangle, \quad (25)$$

$$\Delta_X^{xy} = -g_{xy} \langle v_{Y, \mathbf{k}}^2 e_{Y, \mathbf{k}} e_{Y, -\mathbf{k}} \rangle, \quad (26)$$

$$\Delta_Y^{xy} = -g_{xy} \langle v_{X, \mathbf{k}}^2 e_{X, \mathbf{k}} e_{X, -\mathbf{k}} \rangle, \quad (27)$$

The corresponding self-consistent BCS equations at $T = 0$ are the ones reported in the text, Eq.s (10)-(15). To solve them we introduce polar coordinates and we approximate the orbital factors and the density of states

with their values at the Fermi level for each pocket. This implies that the various integrals can be computed as for example:

$$\begin{aligned}\sum_{\mathbf{k}} u_{X,\mathbf{k}}^2 \frac{\Delta_{X,\mathbf{k}}}{E_{X,\mathbf{k}}} &= \int \frac{kdkd\theta}{(2\pi)^2} u_X^2(\theta) \frac{\Delta_X(\theta)}{\sqrt{\varepsilon_{X,\mathbf{k}}^2 + \Delta_X^2(\theta)}} \\ &= \int \frac{d\varepsilon d\theta}{(2\pi)} N_X(\varepsilon_F, \theta) u_X^2(\theta) \frac{\Delta_X(\theta)}{\sqrt{\varepsilon^2 + \Delta_X^2(\theta)}} \\ &= \int \frac{d\varepsilon d\theta}{(2\pi)} N_X(\varepsilon_F, \theta) u_X^2(\theta) \Delta_X(\theta) \log \frac{\omega_D}{\Delta_X(\theta)}\end{aligned}\quad (28)$$

where we defined $u_X^2(\theta) \equiv u_X^2(k_F(\theta))$ and $\Delta_X(\theta) \equiv \Delta_e^{yz} u_X^2(\theta) + \Delta_x^{xy} u_X^2(\theta)$. The cut-off ω_D represents the range of the spin-mediated pairing interaction, and it has been taken of order of 0.1 eV. The angular dependent density of state is defined as usual as $N_X(\varepsilon_F, \theta) = \int (kdk)/(2\pi) \delta(\varepsilon_F - \varepsilon_{X,\mathbf{k}}) = k_F(\theta)/2\pi |v_F(\theta)|$, where $k_F(\theta)$ and $v_F(\theta)$ are the wavevector and velocity at the Fermi level, respectively. For a parabolic band dispersion $N_X(\varepsilon_F, \theta)$ reduces to an angular-independent constant, as usual. Even though in Eq. (28) the angular integration involves both the orbital factor and the density of states, we checked that the results do not change considerably if the angular-averaged density of states is taken outside the integral. For this reason, accounting separately for the angular averages of the orbital factors alone, as shown in Fig. 3, allows one to have a rough estimate of the numerical results, as discussed in the text. The results of the full numerical self-consistent calculations of Eq.s (10)-(13) are displayed in Fig. 4-5 for $g_X/g_Y = 21$ and $|g_{xy}|/g_X = 0.076$. The numerical values of the band parameters can be found in Supplementary Note 3.

ACKNOWLEDGEMENTS

We acknowledge M. Capone, A. Chubukov and P. Hirschfeld for useful discussions, and M. Capone for critical reading of the manuscript.

COMPETING INTERESTS

The authors declare no competing interests.

AUTHOR CONTRIBUTIONS

L.F. conceived the project with inputs from all coauthors. L.F. and L.B. performed the numerical calculations. All the authors contributed to the data analysis, to the interpretation of the theoretical results and to the writing of the text.

FUNDING

We acknowledge financial support by Italian MAECI under the collaborative Italia-India project SuperTop-PGR04879, by MINECO (Spain) via Grants No.FIS2014-53219-P and by Fundación Ramon Areces. We acknowledge the cost action Nanocoehyri CA16218.

DATA AVAILABILITY

The authors declare that the data supporting the findings of this study are available within the paper and its supplementary notes.

SUPPLEMENTARY MATERIAL

Supplementary Note 1: Band structure

To describe the band structure of FeSe above the superconducting (SC) transition, we adapt the orbital model of ref. 36. The effective band-mass parameters are extracted from ARPES measurements. These values, considerably smaller than the ones predicted by LDA, are usually reproduced remarkably well by DMFT-based calculations⁴⁷. However, both LDA and DMFT fail in the description of the measured Fermi surface (FS), that are always smaller than expected. Such a FS shrinking³⁸, present already well above the nematic transition^{19,51}, and the nematic splitting, can be explained instead within our low-energy approach by accounting for the orbital selective spin fluctuations (OSSF). As detailed in ref. 19, the orbital-dependent self-energy corrections due to the exchange of spin fluctuations at \mathbf{Q}_X and \mathbf{Q}_Y lead in general to a temperature-dependent FS shrinking. Due to the anisotropy of the OSSF in a spin-nematic transition, this results in the nematic orbital splitting below T_s .

To illustrate the model, let us start from the low-energy Hamiltonian around the Γ point in the orbital space:

$$H^\Gamma = \sum_{\mathbf{k},\sigma} \psi_{\mathbf{k}\sigma}^{\Gamma,\dagger} \hat{H}_{0\mathbf{k}}^\Gamma \psi_{\mathbf{k}\sigma}^\Gamma. \quad (29)$$

Here the spinor is defined as $\psi_{\mathbf{k},\sigma}^\Gamma = (c_{yz,\mathbf{k},\sigma}, c_{xz,\mathbf{k},\sigma})$. Taking into account the real part of the isotropic Σ_0^Γ and anisotropic $\Delta\Sigma_h$ components of the self-energy, responsible for the nematic shrinking, one has that:

$$\hat{H}^\Gamma = \begin{pmatrix} h_{0\mathbf{k}}^\Gamma + \Sigma_0^\Gamma + h_{3\mathbf{k}}^\Gamma - \Delta\Sigma_h & h_{1\mathbf{k}}^\Gamma \\ h_{1\mathbf{k}}^\Gamma & h_{0\mathbf{k}}^\Gamma + \Sigma_0^\Gamma - h_{3\mathbf{k}}^\Gamma + \Delta\Sigma_h \end{pmatrix} \quad (30)$$

where the $h_{i,\mathbf{k}}^\Gamma$ components read

$$\begin{aligned}h_{0,\mathbf{k}}^\Gamma &= \varepsilon_\Gamma - a_\Gamma \mathbf{k}^2, \\ h_{1,\mathbf{k}}^\Gamma &= -2b_\Gamma k_x k_y, \\ h_{3,\mathbf{k}}^\Gamma &= b_\Gamma (k_x^2 - k_y^2),\end{aligned}\quad (31)$$

and we defined $\Sigma_0^\Gamma \equiv (\Sigma_{xz}^\Gamma + \Sigma_{yz}^\Gamma)/2$ and $\Delta\Sigma_h \equiv (\Sigma_{xz}^\Gamma - \Sigma_{yz}^\Gamma)/2$. As discussed in refs 19,38 the self-energy corrections are negative at the hole pocket, so the Σ_0^Γ term accounts in general for an uniform shrinking of the pocket, present already in the paramagnetic phase. Below the structural transition temperature, T_S , nematic spin fluctuations induce larger corrections in the \mathbf{Q}_X direction, which translate in a $|\Sigma_{yz}^\Gamma| > |\Sigma_{xz}^\Gamma|$, so that $\Delta\Sigma_h > 0$ (ref.19). Taking into account also the spin-orbit splitting it is easy to see³⁶ that the Hamiltonian (30) gets an additional term $\pm l/2\delta_2$ in the \pm spin sector. As a consequence the eigenvalues defining the bands are given by:

$$\varepsilon_{\Gamma,\mathbf{k},\pm} = h_{0,\mathbf{k}}^\Gamma - |\Sigma_0^\Gamma| \pm \sqrt{h_{1,\mathbf{k}}^{\Gamma^2} + (h_{3,\mathbf{k}}^\Gamma - \Delta\Sigma_h)^2 + (l/2)^2}, \quad (32)$$

where the $+/-$ refers to the outer/inner pocket, respectively. Since the two spin sectors have the same energy dispersion we drop from now on any explicit dependence on the spin index. By introducing the orbital weights:

$$\begin{aligned} u_{\Gamma,\mathbf{k}}^2 &= \frac{1}{2} \left(1 + \frac{h_{3,\mathbf{k}}^\Gamma - \Delta\Sigma_h}{\sqrt{h_{1,\mathbf{k}}^{\Gamma^2} + (h_{3,\mathbf{k}}^\Gamma - \Delta\Sigma_h)^2 + (l/2)^2}} \right) \\ v_{\Gamma,\mathbf{k}}^2 &= \frac{1}{2} \left(1 - \frac{h_{3,\mathbf{k}}^\Gamma - \Delta\Sigma_h}{\sqrt{h_{1,\mathbf{k}}^{\Gamma^2} + (h_{3,\mathbf{k}}^\Gamma - \Delta\Sigma_h)^2 + (l/2)^2}} \right) \end{aligned} \quad (33)$$

one can also define the rotation from the orbital to the band basis

$$\begin{pmatrix} h_{+,\mathbf{k}} \\ h_{-,\mathbf{k}} \end{pmatrix} = \begin{pmatrix} u_{\Gamma,\mathbf{k}} & -v_{\Gamma,\mathbf{k}} \\ v_{\Gamma,\mathbf{k}} & u_{\Gamma,\mathbf{k}} \end{pmatrix} \begin{pmatrix} c_{yz,\mathbf{k}} \\ c_{xz,\mathbf{k}} \end{pmatrix} \quad (34)$$

where h_+^\dagger/h_-^\dagger is the creation operator of a quasiparticle in the outer/inner pocket, respectively. Since in FeSe only the outer pocket crosses the Fermi level, throughout the main text we dropped the $+$ index and we simply referred to $h_{\mathbf{k}}$ and $\varepsilon_{\Gamma,\mathbf{k}}$ as the fermionic operator and bare dispersion of the outer hole pocket. In the paramagnetic phase ($\Delta\Sigma_h = 0$) and in the absence of spin-orbit interaction the two hole bands have a simple parabolic dispersion $\varepsilon_{\Gamma,\mathbf{k},\pm} = \varepsilon_\Gamma - |\Sigma_0^\Gamma| - (a_\Gamma \mp b_\Gamma)\mathbf{k}^2$. In this case the orbital weights only depend on the azimuthal angle θ measured with respect to $k_x = 0$, so that $u_{\Gamma,\mathbf{k}} = \cos\theta$ and $v_{\Gamma,\mathbf{k}} = \sin\theta$. However, the spin-orbit interaction and the nematic splitting mix the two orbital characters, leading to the angular dependence of the orbital weights at the Fermi level shown in Fig. 2d of the main text.

For the X/Y pockets the general structure is analogous to Eq. (29), provided that the spinors are now defined as $\psi_{\mathbf{k}}^X = (c_{yz,\mathbf{k}}, c_{xy,\mathbf{k}})$ and $\psi_{\mathbf{k}}^Y = (c_{xz,\mathbf{k}}, c_{xy,\mathbf{k}})$. In addition, since the xy orbital is not affected by OSSF, one has in general

$$\hat{H}_{\mathbf{k}}^X = \begin{pmatrix} h_{0,\mathbf{k}}^X + \Sigma^X + h_{3,\mathbf{k}}^X & -ih_{2,\mathbf{k}}^X \\ ih_{2,\mathbf{k}}^X & h_{0,\mathbf{k}}^X - h_{3,\mathbf{k}}^X \end{pmatrix} \quad (35)$$

for the X pocket, with

$$\begin{aligned} h_{0,\mathbf{k}}^X &= (h_{yz,\mathbf{k}} + h_{xy,\mathbf{k}})/2 \\ h_{2,\mathbf{k}}^X &= vk_y \\ h_{3,\mathbf{k}}^X &= (h_{yz,\mathbf{k}} - h_{xy,\mathbf{k}})/2 - b(k_x^2 - k_y^2) \end{aligned} \quad (36)$$

where $h_{yz,\mathbf{k}} = -\epsilon_{yz} + a_{yz}\mathbf{k}^2$ and $h_{xy,\mathbf{k}} = -\epsilon_{xy} + a_{xy}\mathbf{k}^2$. Analogous expressions hold for the Y pocket provided that one exchange the role of k_x and k_y , $h_{i,\mathbf{k}}^Y(k_x, k_y) = h_{i,\mathbf{k}}^X(k_y, k_x)$, and Σ_{yz}^X is replaced by Σ_{xz}^Y . At the electron pockets the self-energy corrections are positive, so that the $\Sigma_{yz/xz}^{X/Y}$ terms lead again to an upward shift of the yz/xz orbitals. In the spin-nematic state $\Sigma_{yz}^X > \Sigma_{xz}^Y$ so the yz sector of the X pocket shrinks further and the xz part of the Y pocket expands, see Fig. 1 in the main text. The nematic order parameter at the electron pockets is then defined as $\Delta\Sigma_e = (\Sigma_{yz}^X - \Sigma_{xz}^Y)/2 > 0$. Notice that in our approach the change of sign of the nematic splitting at the Γ and $M = (X, Y)$ point is a natural consequence of the self-energy corrections induced by nematic OSSF, as explained in¹⁹. The X/Y band dispersions are given by

$$\varepsilon_{\mathbf{k},\pm}^{X/Y} = h_{0,\mathbf{k}}^{X/Y} + \Sigma^X/2 \pm \sqrt{h_{2,\mathbf{k}}^{X^2} + (h_{3,\mathbf{k}}^X - \Sigma_{yz}^X/2)^2}, \quad (37)$$

such that $\varepsilon_{\mathbf{k},+}^{X/Y}$ is the electronic band crossing the Fermi level at the X/Y point. The rotation from the orbital to the band basis is defined now as

$$\begin{pmatrix} e_{X,\mathbf{k},+} \\ e_{X,\mathbf{k},-} \end{pmatrix} = \begin{pmatrix} u_{X,\mathbf{k}} & -iv_{X,\mathbf{k}} \\ iv_{X,\mathbf{k}} & u_{X,\mathbf{k}} \end{pmatrix} \begin{pmatrix} c_{yz,\mathbf{k}} \\ c_{xy,\mathbf{k}} \end{pmatrix} \quad (38)$$

with the orbital weights given by

$$\begin{aligned} u_{X,\mathbf{k}}^2 &= \frac{1}{2} \left(1 + \frac{h_{3,\mathbf{k}}^X - \Sigma_{yz}^X/2}{\sqrt{h_{2,\mathbf{k}}^{X^2} + (h_{3,\mathbf{k}}^X - \Sigma_{yz}^X/2)^2}} \right), \\ v_{X,\mathbf{k}}^2 &= \frac{1}{2} \left(1 - \frac{h_{3,\mathbf{k}}^X - \Sigma_{yz}^X/2}{\sqrt{h_{2,\mathbf{k}}^{X^2} + (h_{3,\mathbf{k}}^X - \Sigma_{yz}^X/2)^2}} \right), \end{aligned} \quad (39)$$

At the Y points the definitions are again equivalent, provided that one replaces Σ_{yz}^X with Σ_{xz}^Y and k_x with k_y . As for the hole pocket, we drop the $+$ index and we refer to $e_{X/Y,\mathbf{k}}$ and $\varepsilon_{X/Y,\mathbf{k}}$ as the fermionic operators and energy dispersions of the electronic X/Y pockets. In summary, the notations used in the main text are:

$$\begin{aligned} \varepsilon_{\Gamma,\mathbf{k},+} &\rightarrow \varepsilon_{\Gamma,\mathbf{k}} & h_{+,\mathbf{k}} &\rightarrow h_{\mathbf{k}} & \text{hole pocket} \\ \varepsilon_{X,\mathbf{k},+} &\rightarrow \varepsilon_{X,\mathbf{k}} & e_{X,\mathbf{k},+} &\rightarrow e_{X,\mathbf{k}} & X \text{ pocket} \\ \varepsilon_{Y,\mathbf{k},+} &\rightarrow \varepsilon_{Y,\mathbf{k}} & e_{Y,\mathbf{k},+} &\rightarrow e_{Y,\mathbf{k}} & Y \text{ pocket} \end{aligned}$$

With these definitions in mind the rotation from the orbital to the band basis defined in Eq.s (1)-(3) of the main text are equivalent to Eq. (34) and (38) above.

Finally, we notice that the present low-energy model describes properly the orbital character of the bands up

to energy scale of order of 0.5 eV around the Fermi level, beyond which additional d orbitals should be taken into account⁵². Since both the nematic and SC transition involved much smaller energy scales, the results obtained within the present low-energy approach are expected to be robust with respect to the band-structure description obtained within more sophisticated five- or ten-orbital models.

Supplementary Note 2: Orbital Selective Spin Fluctuations Model

Once established the orbital composition of the low-energy model, one can project the general interacting Hamiltonian including the Hubbard and Hund terms into the low-energy states. As shown in^{32,37} one obtains that the effective low-energy interacting terms can be written as

$$H_{int} = -\frac{\tilde{U}}{2} \sum_{\mathbf{q}} \mathbf{S}_{X/Y}^{yz/xz} \cdot \mathbf{S}_{X/Y}^{yz/xz}. \quad (40)$$

Here \tilde{U} is the intraorbital interaction renormalized at low energy and the intraorbital spin operators connecting hole and electron pocket are given by Eq.s (4)-(5) of the main text, that we rewrite here explicitly including also the contribution of the inner pocket, when present:

$$\mathbf{S}_X^{yz} = \sum_{\mathbf{k}} (u_{\Gamma} h_{+}^{\dagger} + v_{\Gamma} h_{-}^{\dagger}) \vec{\sigma} u_X e_X, \quad (41)$$

$$\mathbf{S}_Y^{xz} = \sum_{\mathbf{k}} (-v_{\Gamma} h_{+}^{\dagger} + u_{\Gamma} h_{-}^{\dagger}) \vec{\sigma} u_Y e_Y, \quad (42)$$

where momentum dependence has been dropped for simplicity. The low-energy interacting Hamiltonian in Eq.(40) defines the OSSF: at low energy the hole pockets at Γ and the X/Y electron pockets share only one orbital, the yz/xz respectively. Thus the spin interactions along x and y has a single orbital character (see Fig 1 in the main text):

$$\begin{aligned} \langle \mathbf{S} \cdot \mathbf{S} \rangle (\mathbf{Q}_X) &\Rightarrow \langle \mathbf{S}_X^{yz} \cdot \mathbf{S}_X^{yz} \rangle \\ \langle \mathbf{S} \cdot \mathbf{S} \rangle (\mathbf{Q}_Y) &\Rightarrow \langle \mathbf{S}_Y^{xz} \cdot \mathbf{S}_Y^{xz} \rangle \end{aligned} \quad (43)$$

By computing self-energy corrections of the orbital states coming from these OSSF one obtains orbital-dependent self-energy corrections, as shown in Eq. (30) and (35) above. In addition, within a spin-nematic scenario the anisotropy of the spin fluctuations at different \mathbf{Q} vectors translates in the nematic splitting $\Delta\Sigma_h$, $\Delta\Sigma_e$ of the orbitals discussed previously. Here we argue that OSSF can also mediate an orbital-selective nematic pairing. The pairing model mediated by OSSF can be easily derived by rewriting the spin-spin interaction terms (40) in the pairing channel, using the projection of the orbital spin operator on the band basis encoded in Eq.s (41)-(42) above. The resulting pairing interaction is given by Eq. (8) of the main text.

Supplementary Note 3: Model parameters for FeSe

We solve self-consistently the set of BCS equations for realistic parameters for the FeSe system in the nematic phase.

Although the physical outcome of this work does not crucially depend on this, instead of using exactly the band parameters of ref. 19, we will adjust them to fit a smaller value of the nematic splitting of the electron pockets reported afterwards in the literature, $\Delta\Sigma_e \simeq 15$ meV^{11,20,21}. When computing self-consistently the spectral function of electrons coupled to spin modes in ref. 19, we included the full frequency-dependent self-energies, thus we also effectively included the quasiparticle weight Z_{spin} due to the orbital-dependent mass renormalization. However, since we checked that Z_{spin} was of order one for the various orbitals, to reduce the number of parameters we decided in the present work to choose directly the band parameters which reproduce the experimental dispersions. This explains the small quantitative differences between the values listed in Table I and those listed in ref. 19. The list of the band parameters appearing in Eq.s (31), (36) and used in the calculations are given in Table I. The spin-orbit coupling is assumed $\lambda = 20$ meV. We use $|\Sigma_{yz/xz}^{\Gamma}| = 70/40$ meV and $\Sigma_{yz/xz}^{X/Y} = 45/15$ meV, in order to have $\Delta\Sigma_{h/e} = 15$ meV.

Γ		X	
ϵ_{Γ}	46	ϵ_{xy}	72
a_{Γ}	263	a_{xy}	93
b_{Γ}	182	b	154
		v	144

TABLE I: Low-energy model parameters for FeSe in the nematic phase at $k_z = 0$. All the parameters are in meV, the k vector is measured in units $1/a \sim 0.375 \text{ \AA}^{-1}$, where $a = a_{FeFe}$ is the lattice constant of the 1-Fe unit cell (so that $\tilde{a} = \sqrt{2}a = 3.77 \text{ \AA}$ is the lattice constant of the 2Fe unit cell).

The u , v , factors defined by Eq.s (33), (39), computed using the above set of parameters, are shown in Fig. 2 of the main text. We reproduce the FS and their orbital distribution as experimentally observed by ARPES at $k_z = 0$ (ref.s 11,19–21,26), with the hole pocket having $k_F^x = 0.056 \text{ \AA}^{-1}$ and $k_F^y = 0.11 \text{ \AA}^{-1}$, the X one $k_F^x = 0.20 \text{ \AA}^{-1}$ and $k_F^y = 0.051$ and the Y , $k_F^x = 0.10$ and $k_F^y = 0.20 \text{ \AA}^{-1}$ in the nematic phase.

Using now the $T = 0$ BCS equations, Eq.s (10)-(15) of the main text, we can fit the experimental data of ref. 22 using the SC couplings as fitting parameters. The results for the orbital SC order parameters, Eq.s (10)-(15), are listed in Table II while in Fig. 4 of the main text we showed the band gaps, Eq.s (16)-(18) of the main text. Notice that assuming isotropic pairing interactions $g_X = g_Y = 1.03$ eV and accounting only for the orbital

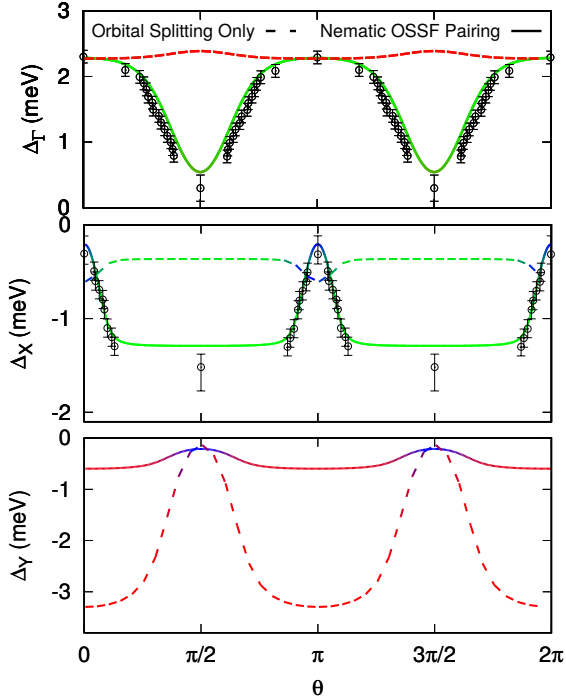


FIG. 6: Numerical results for the band gaps on the Γ (top), X (middle) and Y (bottom) pocket obtained considering a larger nematic splitting at M , $\Delta\Sigma_e = 20$ meV.

splitting effects, encoded in the u, v factors, the SC gap at Γ presents opposite anisotropy with respect to the one found in the experiment. On the other hand, considering nematic pairing, $g_X/g_Y = 21$, with $g_X = 5.88$ eV $>$ $g_Y = 0.28$ eV we reproduce both the absolute values and the angular modulation of the observed gap at Γ and X . For sake of completeness in Fig. 4 we show the results obtained including the xy -pairing channel. We use $g_{xy} = -0.45$ eV in order to reproduce the experimental data from ref. 22. The inclusion of such contribution does not affect the discussion above. Notice that our results are rather robust with respect to small variations of the band parameters and nematic splitting. For example, a larger nematic splitting $\Delta\Sigma_e = 20$ at M as initially estimated in ref. 19, would not alter our results, see Fig. 6. The only difference is that in this case one has a larger gain from the orbital ordering at M , so that the experimental data are reproduced with a slightly smaller nematic pairing $g_X/g_Y = 19$.

Δ_h^{yz}	Δ_h^{xz}	Δ_e^{yz}	Δ_e^{xz}	Δ_X^{xy}	Δ_Y^{xy}
15.71	0.19	-1.46	-0.71	-0.20	-0.23

TABLE II: $T = 0$ orbital SC order parameters (in meV) of the band gap shown in Fig 4 of the main text.

It is interesting to compare the value of the anisotropy obtained here with the anisotropy of the OSSF extracted from the analysis of the shrinking effect in ref. 19. In ref.

19 the spectral function of the spin modes along the two directions has been modelled as:

$$B_{X/Y}(\omega) = \frac{1}{\pi} \frac{\omega\omega_0}{\omega_{X/Y}^2 + \omega^2}. \quad (44)$$

While at RPA level the spin modes are always degenerate, taking into account spin-spin interactions beyond Gaussian level^{32,53} one can show that below T_S spin fluctuations break the Z_2 Ising degeneracy and they become stronger at a given \mathbf{Q} vector. This is encoded in Eq. (44) above with two anisotropic masses $\omega_{X/Y}$ below T_S . The analysis of the orbital ordering induced by OSSF discussed in¹⁹ and outlined above shows that below T_S one should then have stronger spin fluctuations at \mathbf{Q}_X , which implies $\omega_X < \omega_Y$ and $V_X > V_Y$, where $V_{X/Y}$ is the coupling of the fermions to the spin modes. The strength of the pairing interaction is given by the product of the real part $\chi'_{X/Y}(\omega = 0)$ of the spin-fluctuation propagator at $\omega = 0$ times the spin-mode coupling $V_{X/Y}$. Using then the Kramers-Kronig relation of χ' to the spectral function (44) we get:

$$\begin{aligned} g_{X/Y} &\propto V_{X/Y} \chi'_{X/Y}(\omega = 0) = V_{X/Y} \int d\omega \frac{B_{X/Y}(\omega)}{\omega} = \\ &= V_{X/Y} \frac{\omega_0}{\omega_{X/Y}} \end{aligned} \quad (45)$$

The analysis of ARPES measurements performed in ref. 19 gives at $T > T_c$ $\omega_Y/\omega_X = 1.6$ and $V_X/V_Y = 8$. Here we used, in the notation of ref. 19, the values of the coupling $V_{X/Y}^{eh}$. With these numbers we obtain $g_X/g_Y = 13.4$, a ratio of the same order of magnitude of what we extracted from the gap anisotropy $g_X/g_Y = 21$. Notice that the present estimate does not take into account the feedback of the SC order on the spin modes and could explain the difference between the two results. Such a full self-consistent treatment is beyond the scope of the present manuscript and will be addressed in a future work.

Let us finally address the issue of the k_z gap dependence. As discussed in the main text, a crucial difference when moving from $k_z = 0$ to $k_z = \pi$ is that the orbital character of the hole pocket changes considerably. Since all the FS pockets expand^{24,25,28}, the effect of the nematic order is less dramatic on the hole pocket, with the consequence that it retains full yz character at $\theta = 0$ ²⁵. This has already a profound impact on the hole-gap anisotropy, as recently pointed out in ref. 35. To highlight the effect of the change of orbital weights on the hole pocket at Z we analyze the BCS solution using a set of realistic band parameters for the Z -pocket as listed in Table III.

In the absence of a detailed comparison with the band structure above T_S as done in ref. 19, we already include in ϵ_Z the effect of the isotropic shrinking, $(\Sigma_{yz}^\Gamma + \Sigma_{xz}^\Gamma)/2$, and consider separately a further nematic splitting $\Delta\Sigma_h = 10$ meV. In Fig. 7 we show the FS shape

Z	
ϵ_Z	26
a_Z	473
b_Z	264

TABLE III: Low-energy model parameters for the hole-pocket at $k_z = \pi$ in the nematic phase.

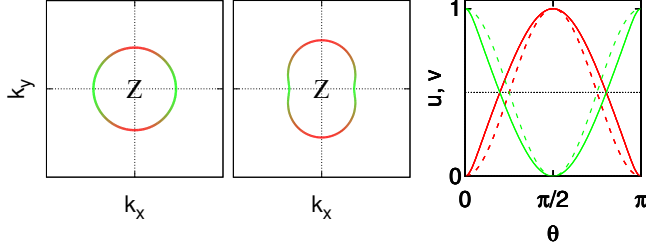


FIG. 7: $k_z = \pi$ cut of the FS FeSe in the (a) paramagnetic and (b) nematic phase. The colors represent the main orbital character. (c) Orbital component amplitude of the FS as a function of the azimuthal angle theta in the tetragonal (dashed lines) and nematic phase (solid lines)

and composition of the Z pocket in both the paramagnetic and nematic phase. Notice that even below T_s , the large elliptical Z pocket, $k_F^x = 0.10 \text{ \AA}^{-1}$ and $k_F^y = 0.15 \text{ \AA}^{-1}$, retains a marked yz character at $\theta = 0$ in agreement with the ARPES measurements^{24,25,28}. Moreover given this band structure, the inclusion of a finite spin-orbit coupling does not lead to any significant change, and the u_Z, v_Z , factors defined as Eq.s (33), (39) scale approximately as $\cos \theta$ and $\sin \theta$ even below T_s .

Solving the BCS equation in this case one can easily check that, contrary to what found at $k_z = 0$, $\langle u_Z^4 \rangle \sim \langle v_Z^4 \rangle$, so that the increase of the $\langle u_X^4 \rangle$ factor over the $\langle u_Y^4 \rangle$ in the nematic phase is enough to have $\Delta_h^{yz} > \Delta_h^{xz}$. In this case already without nematic pairing one has a larger gap value at $\theta = 0$, as observed indeed in ref. 35 (see also Fig 5 in the main text). As a con-

sequence, if one retains instead the pairing anisotropy g_X/g_Y extracted from the fitting of the $k_z = 0$ gaps the anisotropic effect due to the nematic pairing is amplified now by the orbital factors that cooperates to give the same gap modulation. As a result we would get larger gap values and larger anisotropy when moving from the Γ to the Z pocket. Recent ARPES experiments investigated the SC gaps at $k_z = \pi$ ^{24–26,28}. While all the experiments confirm the in-plane anisotropy of the gap of the hole-pocket, with a larger gap value at $\theta = 0$, the various reports are somehow in disagreement on the k_z dependence of the gap-magnitude. In fact in refs 24,28 the absolute value of the gap and its anisotropy are found to be larger at $k_z = \pi$, while in refs 25,26 the authors claimed a decreasing of the gap magnitude when moving from the Γ to the Z pocket. The present situation calls for a more detailed experimental analysis and specific theoretical studies involving a 3D modeling of the band structure. As a matter of fact, details of the 3D band model could change the estimate of the magnitude of the gaps at different k_z , influencing the orbital ordering effects and the balance between such mechanism and the nematic pairing one. For example, in ref. 35 the authors obtain a larger anisotropy $\Delta_{max}/\Delta_{min}$ at the Z pocket than in our case. This is possibly due to a much larger suppression of xz character at the Y pocket in their model, leading to a larger $\langle u_X^4 \rangle \gg \langle u_Y^4 \rangle$ anisotropy at the electron pockets. Unfortunately, the controversy on the observation of the Y pocket in ARPES^{26,28} does not allow us to disentangle this issue experimentally. Finally, notice that the authors of ref. 35 do not solve the self-consistent equations at $T = 0$, as we do, but the linearized ones near T_c . Since in a multiband system the ratios of the gaps in the various bands depend on temperature, one cannot trivially compare those results with the one discussed in the present manuscript. Nonetheless, the main qualitative findings, and in particular the wrong gap anisotropy found at Γ without nematic pairing, hold in both works, apart from possible quantitative differences.

* Electronic address: laura.fanfarillo@sissa.it

¹ Mazin, I. I., Singh, D. J., Johannes, M. D. & Du, M. H. Unconventional superconductivity with a sign reversal in the order parameter of $\text{LaFeAsO}_{1-x}\text{F}_x$. *Phys. Rev. Lett.* **101**, 057003 (2008).

² Kuroki, K. et al. Unconventional pairing originating from the disconnected Fermi surfaces of superconducting $\text{LaFeAsO}_{1-x}\text{F}_x$. *Phys. Rev. Lett.* **101**, 087004 (2008).

³ Chubukov, A. Pairing mechanism in Fe-based superconductors. *Annual Review of Condensed Matter Physics* **3**, 57–92 (2012).

⁴ Platt, C., Hanke, W. & Thomale, R. Functional renormalization group for multi-orbital Fermi surface instabilities. *Advances in Physics* **62**, 453–562 (2013).

⁵ Hirschfeld, P. J. Using gap symmetry and structure to reveal the pairing mechanism in Fe-based superconductors. *Comptes Rendus Physique* **17**, 197 – 231 (2016). Iron-based superconductors / Supraconducteurs à base de fer.

⁶ Rahn, M. C., Ewings, R. A., Sedlmaier, S. J., Clarke, S. J. & Boothroyd, A. T. Strong $(\pi, 0)$ spin fluctuations in β -FeSe observed by neutron spectroscopy. *Phys. Rev. B* **91**, 180501 (2015).

⁷ Wang, Q. et al. Strong interplay between stripe spin fluctuations, nematicity and superconductivity in FeSe. *Nature materials* **15**, 159 (2016).

⁸ Wang, Q. et al. Magnetic ground state of FeSe. *Nature communications* **7**, 12182 (2016).

⁹ He, M. et al. Evidence for short-range magnetic order in

- the nematic phase of FeSe from anisotropic in-plane magnetostriction and susceptibility measurements. *Phys. Rev. B* **97**, 104107 (2018).
- ¹⁰ Wiecki, P. et al. Persistent correlation between superconductivity and antiferromagnetic fluctuations near a nematic quantum critical point in $\text{FeSe}_{1-x}\text{S}_x$. *Phys. Rev. B* **98**, 020507 (2018).
 - ¹¹ Coldea, A. I. & Watson, M. D. The key ingredients of the electronic structure of FeSe. *Annual Review of Condensed Matter Physics* **9**, 125–146 (2018).
 - ¹² Gallais, Y. & Paul, I. Charge nematicity and electronic raman scattering in iron-based superconductors. *Comptes Rendus Physique* **17**, 113 – 139 (2016). Iron-based superconductors / Supraconducteurs à base de fer.
 - ¹³ Shimojima, T. et al. Lifting of xz/yz orbital degeneracy at the structural transition in detwinned FeSe. *Phys. Rev. B* **90**, 121111 (2014).
 - ¹⁴ Nakayama, K. et al. Reconstruction of band structure induced by electronic nematicity in an FeSe superconductor. *Phys. Rev. Lett.* **113**, 237001 (2014).
 - ¹⁵ Watson, M. D., et al. Emergence of the nematic electronic state in FeSe. *Phys. Rev. B* **91**, 155106 (2015).
 - ¹⁶ Zhang, P. et al. Observation of two distinct d_{xz}/d_{yz} band splittings in FeSe. *Phys. Rev. B* **91**, 214503 (2015).
 - ¹⁷ Suzuki, Y. et al. Momentum-dependent sign inversion of orbital order in superconducting FeSe. *Phys. Rev. B* **92**, 205117 (2015).
 - ¹⁸ Zhang, Y. et al. Distinctive orbital anisotropy observed in the nematic state of a FeSe thin film. *Phys. Rev. B* **94**, 115153 (2016).
 - ¹⁹ Fanfarillo, L. et al. Orbital-dependent Fermi surface shrinking as a fingerprint of nematicity in FeSe. *Phys. Rev. B* **94**, 155138 (2016).
 - ²⁰ Fedorov, A. et al. Effect of nematic ordering on electronic structure of FeSe. *Scientific reports* **6**, 36834 (2016).
 - ²¹ Watson, M. D., Haghighirad, A. A., Rhodes, L. C., Hoesch, M. & Kim, T. K. Electronic anisotropies revealed by detwinned angle-resolved photo-emission spectroscopy measurements of FeSe. **19**, 103021 (2017).
 - ²² Sprau, P. O. et al. Discovery of orbital-selective cooper pairing in FeSe. *Science* **357**, 75–80 (2017).
 - ²³ Song, C.-L. et al. Direct observation of nodes and twofold symmetry in FeSe superconductor. *Science* **332**, 1410–1413 (2011).
 - ²⁴ Xu, H. C. et al. Highly anisotropic and twofold symmetric superconducting gap in nematically ordered $\text{FeSe}_{0.93}\text{S}_{0.07}$. *Phys. Rev. Lett.* **117**, 157003 (2016).
 - ²⁵ Hashimoto, T. et al. Superconducting gap anisotropy sensitive to nematic domains in FeSe. *Nature communications* **9**, 282 (2018).
 - ²⁶ Rhodes, L. C. et al. Scaling of the superconducting gap with orbital character in FeSe. *arXiv preprint arXiv:1804.01436* (2018).
 - ²⁷ Liu, D. et al. Orbital origin of extremely anisotropic superconducting gap in nematic phase of FeSe superconductor. *Phys. Rev. X* **8**, 031033 (2018).
 - ²⁸ Kushnirenko, Y. S. et al. Three-dimensional superconducting gap in FeSe from angle-resolved photoemission spectroscopy. *Phys. Rev. B* **97**, 180501 (2018).
 - ²⁹ Sato, Y. et al. Abrupt change of the superconducting gap structure at the nematic critical point in $\text{FeSe}_{1-x}\text{S}_x$. *Proceedings of the National Academy of Sciences* (2018).
 - ³⁰ Sun, Y. et al. Gap structure of FeSe determined by angle-resolved specific heat measurements in applied rotating magnetic field. *Phys. Rev. B* **96**, 220505 (2017).
 - ³¹ Kreisel, A. et al. Orbital selective pairing and gap structures of iron-based superconductors. *Phys. Rev. B* **95**, 174504 (2017).
 - ³² Fanfarillo, L., Benfatto, L. & Valenzuela, B. Orbital mismatch boosting nematic instability in iron-based superconductors. *Phys. Rev. B* **97**, 121109 (2018).
 - ³³ Fernandez-Martin, R., Fanfarillo, L., Benfatto, L. & Valenzuela, B. Dc conductivity anisotropy by orbital selective spin fluctuations in the nematic phase of iron superconductors. *arXiv preprint arXiv:1804.07293* (2018).
 - ³⁴ Fernandes, R., Chubukov, A. & Schmalian, J. What drives nematic order in iron-based superconductors? *Nature physics* **10**, 97 (2014).
 - ³⁵ Kang, J., Fernandes, R. M. & Chubukov, A. Superconductivity in FeSe: The role of nematic order. *Phys. Rev. Lett.* **120**, 267001 (2018).
 - ³⁶ Cvetkovic, V. & Vafeek, O. Space group symmetry, spin-orbit coupling, and the low-energy effective hamiltonian for iron-based superconductors. *Phys. Rev. B* **88**, 134510 (2013).
 - ³⁷ Fanfarillo, L., Cortijo, A. & Valenzuela, B. Spin-orbital interplay and topology in the nematic phase of iron pnictides. *Phys. Rev. B* **91**, 214515 (2015).
 - ³⁸ Ortenzi, L., Cappelluti, E., Benfatto, L. & Pietronero, L. Fermi-surface shrinking and interband coupling in iron-based pnictides. *Phys. Rev. Lett.* **103**, 046404 (2009).
 - ³⁹ Coldea, A. I. et al. Fermi surface of superconducting LaFePO determined from quantum oscillations. *Phys. Rev. Lett.* **101**, 216402 (2008).
 - ⁴⁰ Brouet, V. et al. Large temperature dependence of the number of carriers in co-doped BaFe_2As_2 . *Phys. Rev. Lett.* **110**, 167002 (2013).
 - ⁴¹ Kemper, A. F. et al. Sensitivity of the superconducting state and magnetic susceptibility to key aspects of electronic structure in ferropnictides. *New Journal of Physics* **12**, 073030 (2010).
 - ⁴² Hardy, F. et al. Nodal gaps in the nematic superconductor FeSe from heat capacity. *arXiv preprint arXiv:1807.07907* (2018).
 - ⁴³ Fanfarillo, L. & Benfatto, L. Anisotropy of the superconducting fluctuations in multiband superconductors: the case of LiFeAs . *Superconductor Science and Technology* **27**, 124009 (2014).
 - ⁴⁴ Rullier-Albenque, F., Colson, D., Forget, A. & Alloul, H. Multiorbital effects on the transport and the superconducting fluctuations in LiFeAs . *Phys. Rev. Lett.* **109**, 187005 (2012).
 - ⁴⁵ Kreisel, A., Andersen, B. M. & Hirschfeld, P. Itinerant approach to magnetic neutron scattering of FeSe: effect of orbital selectivity. *arXiv preprint arXiv:1807.09482* (2018).
 - ⁴⁶ de’Medici, L., Georges, A. & Biermann, S. Orbital-selective mott transition in multiband systems: Slave-spin representation and dynamical mean-field theory. *Phys. Rev. B* **72**, 205124 (2005).
 - ⁴⁷ de’ Medici, L., Giovannetti, G. & Capone, M. Selective mott physics as a key to iron superconductors. *Phys. Rev. Lett.* **112**, 177001 (2014).
 - ⁴⁸ Fanfarillo, L., Giovannetti, G., Capone, M. & Bascones, E. Nematicity at the hund’s metal crossover in iron superconductors. *Phys. Rev. B* **95**, 144511 (2017).
 - ⁴⁹ Kostin, A. et al. Imaging orbital-selective quasiparticles in the hund’s metal state of FeSe. *Nature materials* **17**, 869–874 (2018).

- ⁵⁰ Hu, H., Yu, R., Nica, E. M., Zhu, J.-X. & Si, Q. Orbital-selective superconductivity in the nematic phase of FeSe. arXiv preprint arXiv:1805.05915 (2018).
- ⁵¹ Kushnirenko, Y. S. et al. Anomalous temperature evolution of the electronic structure of fese. *Phys. Rev. B* **96**, 100504 (2017).
- ⁵² Fernandes, R. M. & Chubukov, A. V. Low-energy microscopic models for iron-based superconductors: a review. *Reports on Progress in Physics* **80**, 014503 (2017).
- ⁵³ Fernandes, R. M., Chubukov, A. V., Knolle, J., Eremin, I. & Schmalian, J. Preemptive nematic order, pseudogap, and orbital order in the iron pnictides. *Phys. Rev. B* **85**, 024534 (2012).